

Efficient model-free deconvolution of measured femtosecond kinetic data using a genetic algorithm

Ernő Keszei^{a*}

Due to the uncertainty relation between the temporal and spectral widths of a laser pulse, sufficient selectivity in excitation and detection energy does not allow much shorter pulses in a femtosecond pump-probe experiment than about 100 fs. Many ultrafast chemical processes have comparable characteristic times, so the results of these experiments are severely distorted by convolution of the kinetic response function with the pulses used. If we do not know the underlying photochemical and kinetic model, the only way to overcome the limitation in time resolution due to convolution is to perform a model-free deconvolution. Most existing deconvolution methods—even after specifically adapted to femtochemical experimental data (Bányász Á, Keszei E. Nonparametric deconvolution of femtosecond kinetic data. *J. Phys. Chem. A* 2006; 110: 6192–6207)—do not provide a smooth deconvolved data set that could be used for unbiased statistical inference. Here, we report an efficient model-free deconvolution method that enhances temporal resolution and improves statistical inference from measured pump-probe data, using a genetic algorithm (GA). The proposed algorithm enables to create a fairly good initial population and uses highly efficient population dynamics to result in individuals who represent excellent solutions of the deconvolution problem without noise amplification, even in the case of a sharp initial step-like rise of the signal. The treatments of both synthetic and experimental data are supporting the outstanding applicability of the proposed deconvolution method. Copyright © 2009 John Wiley & Sons, Ltd.

Keywords: deconvolution; genetic algorithm; transient signals; femtochemistry

1. INTRODUCTION

Chemical applications of deconvolution started in the early thirties of the 20th century to sharpen convolved experimental spectral lines [1]. With the development of chromatography, deconvolution methods have also been used essentially for the same purpose, to get a better resolution of components [2–3]. The need for deconvolution also emerged in the evaluation of pulse radiolysis, flash photolysis and later laser photolysis results, when studied kinetic processes were so fast that reaction times were comparable to the temporal width of the pulse or lamp signals (see e.g. Reference [4]). However, the aim of deconvolution in these kinetic applications was not a sharpening of the signal, but the exact reconstruction of a distortion-free kinetic response function. A number of methods have been used ever since to get the deconvolved kinetic signals in different applications [5–8]. With the availability of ultrafast pulsed lasers, femtochemistry has been developed [9–11], where the time resolution enables the very detection of the transition state in an elementary reaction. Due to several limiting factors, applied laser pulses have typically a temporal width which is comparable to the characteristic time of many interesting elementary reactions. As a consequence, convolution of the measured kinetic signal with the laser pulses used is an inevitable source of signal distortion in most femtochemical experiments.

In previous publications [12–14], we have dealt with several classical methods of deconvolution either based on inverse filtering via Fourier transformation, or on different iterative procedures. Methods reported in these papers resulted in a quite

good quality of deconvolution, but a sufficiently low level of noise in the deconvolved data could only have been achieved if some smoothing was also used, which in turn introduced a small bias due to the lack of high frequency components as a consequence of additional smoothing. Though this phenomenon is quite common when using classical deconvolution methods, it makes subsequent statistical inference also biased. As it has been stated, an appropriate use of *ad hoc* corrections based on the actual experimental data can largely improve the quality of the deconvolved data set by diminishing the bias. This experience led us to explore the promising group of genetic algorithms (GAs), where the wide range of variability of operators enables specific 'shaping' of deconvolution results.

In this paper we describe the application of a modified GA that we successfully use for nonparametric deconvolution of femtosecond kinetic traces. Though GAs are not widely used for deconvolution purposes yet, they are rather promising candidates to be used more frequently in the near future. The few applications in the literature include image processing [15–17],

* Correspondence to: E. Keszei, Department of Physical Chemistry and Reaction Kinetics Laboratory, Eötvös University, 1518 Budapest 112, PO Box 32, Hungary.
E-mail: keszei@chem.elte.hu

a E. Keszei
Department of Physical Chemistry and Reaction Kinetics Laboratory, Eötvös University, 1518 Budapest 112, PO Box 32, Hungary

spectroscopy [18,19], chromatography [20–23] and pharmacokinetics [24].

The rest of the paper is organised as follows. In the next section, we briefly explain the details of the procedure of ultrafast laser kinetic measurements leading to the detected convolved kinetic traces. In Section 3 we outline the mathematical background of nonparametric deconvolution and summarise previous results and their shortcomings in the deconvolution of transient kinetic signals. In Section 4 we describe the implementation of the GA used. Section 5 gives details of results obtained deconvolving simulated and experimental femtochemical data, followed by a summary in Section 6.

2. CONVOLUTION OF THE DETECTED FEMTOSECOND PUMP-PROBE SIGNALS

A detailed description of the most typical kinetic experiment in femtochemistry—the pump-probe method—can be found in a previous publication [14]. Here we only give a brief formulation of the detected transient signal. The pump pulse excites the sample proportional to its intensity $I_g(t)$ at a given time t . As a consequence, the instantaneous kinetic response $c(t)$ of the sample will become the convolution

$$c_g(t) = \int_{-\infty}^{\infty} c(x)I_g(t-x)dx \equiv c \otimes I_g \quad (1)$$

where x is a dummy variable of time dimension. The pump pulse is followed after a delay τ —controlled by a variable optical path difference between the two pulses—by the probe pulse $I_m^0(t+\tau)$, which is normalised so that for any τ

$$\int_{-\infty}^{\infty} I_m^0(t+\tau)dt = 1 \quad (2)$$

if there is no excitation by the pump pulse prior to the probe pulse. The intensity of the probe pulse diminishes while propagating within the excited sample according to Beer's law

$$I_m(t+\tau) = I_m^0(t+\tau)e^{-Ac_g(t)} \quad (3)$$

where $A = \varepsilon / \ln 10$, ε being the decadic molar absorptivity of the species that has been formed due to the pump pulse, and l is the path length in the sample. If the exponent $Ac_g(t)$ is close to zero, the exponential can be replaced by its first-order Taylor polynomial $1 - Ac_g(t)$, with a maximum error of $(Ac_g(t))^2/2$. The detector—whose electronics is slow compared to the sub-picosecond pulse width—measures a signal which is proportional to the time-integral of the pulse, so the detected reference signal (before excitation) is

$$S^0 = K \int_{-\infty}^{\infty} I_m^0(t+\tau)dt = K \quad (4)$$

while after excitation, it is

$$S = K \int_{-\infty}^{\infty} I_m(t+\tau)dt \approx K \int_{-\infty}^{\infty} I_m^0(t+\tau)[1 - Ac_g(t)]dt \quad (5)$$

The output of the measurement is the so-called differential optical density, which makes the proportionality constant K cancel:

$$\Delta OD(\tau) = \frac{S^0 - S}{S^0} \approx \int_{-\infty}^{\infty} I_m^0(t+\tau)Ac_g(t)dt \quad (6)$$

Let us substitute $c_g(t)$ from Equation (1) into the above expression:

$$\Delta OD(\tau) \approx A \int_{-\infty}^{\infty} I_m^0(t+\tau) \left[\int_{-\infty}^{\infty} c(x)I_g(t-x)dx \right] dt \quad (7)$$

Rearranging and changing the order of integration, we get

$$\Delta OD(\tau) \approx A \int_{-\infty}^{\infty} c(x) \left[\int_{-\infty}^{\infty} I_m^0(t+\tau)I_g(t-x)dt \right] dx \quad (8)$$

Let us rewrite this equation by inverting the time axis of both the pump and the probe pulses according to

$$\tilde{I}_g(-t) = I_g(t) \text{ and } \tilde{I}_m^0(-t+\tau) = I_m^0(t+\tau) \quad (9)$$

which corresponds physically to change the direction of time without changing the direction of the delay. Substituting these functions into Equation (8), we get

$$\Delta OD(\tau) \approx A \int_{-\infty}^{\infty} c(x) \left[\int_{-\infty}^{\infty} \tilde{I}_m^0(-t+\tau)\tilde{I}_g(x-t)dt \right] dx \quad (10)$$

Introducing variable $y = x - t$, this can be written as

$$\Delta OD(\tau) \approx A \int_{-\infty}^{\infty} c(x) \left[\int_{-\infty}^{\infty} \tilde{I}_m^0(y+\tau-x)\tilde{I}_g(y)dy \right] dx \quad (11)$$

As the correlation of two functions f and g can be written as

$$\text{corr}[f, g](t) \equiv \int_{-\infty}^{\infty} f(x+t)g(x)dx \quad (12)$$

we can rewrite Equation (11) in the form

$$\Delta OD(\tau) \approx A \int_{-\infty}^{\infty} c(x)\text{corr}[\tilde{I}_m^0, \tilde{I}_g](\tau-x)dx \quad (13)$$

which is a convolution:

$$\Delta OD(\tau) \approx \text{corr}[\tilde{I}_m^0, \tilde{I}_g] \otimes (c \varepsilon l \ln 10) \quad (14)$$

In this latter expression, the correlation of the inverted time axis pump and probe functions is the same as the correlation of the original pump and probe (usually called as the *effective pulse*

or *instrument response function*, IRF), while the transient kinetic function to be determined is $(\varepsilon/\ln 10)c$. If there are more than one transient species formed due to the excitation absorbing at the probe wavelength, we should sum the contributions of all the n absorbing species writing $\sum_{k=1}^n \varepsilon_k I c_k$ in place of $\varepsilon I c$. In case of fluorescence detection, the fluorescence signal is proportional either to the absorbed probe pulse intensity that reexcites the transient species, or to the gating pulse intensity. As a result, the only difference to Equation (14) is the appearance of a proportionality constant.

Introducing the notation of image processing, let us denote the IRF as the *spread* s , and the transient kinetic function the *object* o . The *image* i is the detected (distorted) differential optical density. Hereafter we use the equation equivalent to Equation (14) in the form

$$i = o \otimes s \quad (15)$$

which represents the integral equation

$$i(\tau) = \int_{-\infty}^{\infty} o(t)s(\tau - t)dt \quad (16)$$

to describe the detected transient signal.

Many elementary reactions are typically complete within a picosecond, while the effective pulse often has a width comparable to the characteristic time of the reaction. This is due to the uncertainty relation which sets a limit to the temporal width of the pulse if we prescribe its spectral width [25]. The narrow spectral width is necessary for a selective excitation and detection of the chosen species. The usual spectral width of about 5 nm in the visible range corresponds to about 100 fs transform limited (minimal) pulse width. As a consequence, sub-picosecond kinetic traces are usually heavily distorted by the convolution described above. That's why it is necessary to deconvolve most of the femtochemical transient signals while performing a kinetic interpretation of the observed data.

3. DECONVOLUTION OF TRANSIENT SIGNALS

In an actual measurement, a discretised data set i_m is registered with some experimental error. (Even if there weren't for these errors, numerical truncation by the A/D converter would result in rounding errors.) To get the undistorted kinetic data set o_m , we should know the spread function s or the discretised s_m data set and solve the integral Equation (16). The problem with solving it is that it has an infinite number of (mostly spurious) solutions, from which we should find the physically acceptable unique undistorted data set. Existing deconvolution methods typically treat strictly periodic data (whose final datum is the same as the first one), and give at least slightly biased deconvolved result due to the necessary damping of high frequency oscillations that occur during deconvolution [14,26]. A widely used method to circumvent ambiguities of deconvolution is to use the convolved model function to fit the experimental image data, thereby estimating the parameters of the photophysical and kinetic model; which is called *reconvolution*. Apart from the fact that many reactive systems are too much complicated to have an established kinetic model (e.g. proteins or DNA), the inevitable correlation between pulse parameters and kinetic parameters

also introduces some bias in the estimation, which can be avoided using nonparametric deconvolution prior to parameter estimation.

In a previous publication [14] we thoroughly investigated several classical deconvolution methods used in signal processing, image processing, spectroscopy, chromatography and chemical kinetics. We have successfully applied inverse filtering methods (based on Fourier transforms) using additional filters and avoiding the problem of non-periodicity of data sets, and also iterative methods to deconvolve femtosecond kinetic data. Synthetic data sets were analysed and parameters of the model function obtained from estimation using the deconvolved data were compared to the known parameters. Comparing estimated parameters to those obtained by reconvolution—where the information provided by the knowledge of the true model function was used during the virtual deconvolution—it turned out that there was a smaller bias present in the parameters obtained after model-free deconvolution than in the reconvolution estimates. This supports that a model-free deconvolution followed by fitting the known model function to the deconvolved data set effectively diminishes the bias in most estimated parameters. The reason for this is that using reconvolution, there is a need for an additional parameter, the 'zero time' of the effective pulse, which increases the number of degrees of freedom in the statistical inference and introduces additional correlations within the estimated parameters, thus enabling an extra bias.

Despite of the mentioned qualities of model-free deconvolution, there was always an inevitable bias present in the deconvolved data set due to the necessary noise-damping, which resulted in an amplification of low-frequency components in the signal. Optimal results were obtained by a trade-off between noise suppression and low-frequency distortion. Improvement could be made to diminish this bias by using *ad hoc* corrections which made use of specific properties of actual image functions, using appropriate constraints in the deconvolution. This suggested to try GAs for model-free deconvolution. GAs are very much flexible with respect to the use of genetic operators that could treat many specific features of different transient shapes.

4. DECONVOLUTION USING GENETIC ALGORITHMS

The idea of using GAs for mathematical purposes came from population genetics and breeding sciences. It has been first used and thoroughly investigated by Holland [27], and slowly gained a wide variety of different applications, also in the field of optimisation. There are comprehensive printed monographs [28,29] as well as easy-to-read short introductions available on the web [30] to read about the basic method and its variants. We only summarise here the very basics before describing its use for deconvolution and the actual implementation we use.

The solution of a problem is represented as an '*individual*', and a certain number of individuals form a *population*. The *fitness* of each individual is calculated which measures the quality of the solution. Individuals with high fitness are *selected* to mate, and reproduction of individuals is done by *crossover* of these parents, thus *inheriting* some features from both of them. After crossover, each *offspring* has a chance to suffer *mutation*, and then the *new generation* is selected. Members of the next generation can be

selected either from parents and offspring, or only from the offspring. If the very fittest parent(s) are only selected in addition to offspring, this is called an *elitist selection*, which guarantees a monotonic improvement of the fittest individual from generation to generation. A GA starts with the selection of an *initial population*, and continues with iteration steps resulting in new generations. The iteration is stopped either by the fulfilment of some convergence criterion, or after a predetermined number of generations. The best fit individual—called the *winner*—is selected as the solution of the problem.

In the 'classical' version of GA, individuals have been represented as a binary string, which coded either the complete solution, or parameters to be optimised. These strings were considered as the genetic material of individuals, or *chromosomes*, while the bits of the string as *genes*, having two different *alleles*, 0 or 1. As it is sometimes problematic to represent a solution in the form of binary strings, for numerical optimisation purposes, *floating point* coding is usually used, which allows virtually infinite number of alleles. Classical (binary) genetic operators have accordingly been also replaced by *arithmetic* operators. The 'art' of using GA's is in finding a suitable representation or data structure for the solution and using genetic operators that can explore the *solution space* in an efficient way, avoiding local optima and converging quickly to the global optimum.

Deconvolution methods described in the literature use different representations and a variety of genetic operators. While binary coding and classical binary crossover and mutation are appropriate for processing black and white images [16], much more 'tricky' encoding and operators should be used to deconvolve measured kinetic signals [24]. Generation of the initial population may also be critical. One method is the completely random generation of the first individuals, while a careful generation of already fit individuals is sometimes important.

To deconvolve femtosecond kinetic data, we should deal with the same problems while using a GA as with other methods: avoid an amplification of the experimental noise as well as oversmoothing which results in low frequency 'wavy' distortion. The non-periodic nature and sudden stepwise changes should also be reconstructed without distortion. We have found that the above needs cannot be fulfilled if we start the 'breeding' with a randomly generated initial population. Therefore, the first task is to create individuals who already reflect some useful properties of a good solution.

Before discussing the detailed algorithm, we show here a schematic description of the procedure we use:

1. Start with the measured (convolved) data set; apply creation operators using random factors to generate a population of n chromosomes (candidate solutions of the convolution equation) each containing the same number of data as the measured data set.
2. Calculate the fitness of each chromosome in the population.
3. Repeat Steps (a)–(c) until $n-1$ offspring have been created:
 - (a) Select a pair of parent chromosomes from the current population with a probability of selection proportional to their fitness. Selection is done with replacement, i.e. the same chromosome can be selected more than once to become a parent.
 - (b) Cross over the pair by averaging the corresponding data.
 - (c) Mutate the average with a probability P_m (the mutation probability or mutation rate) by adding a discretised random Gaussian to the data set.

4. Replace the current population with the new population by adding the best fit individual of the previous population as the n th individual.
5. If the termination condition is not fulfilled, go to Step 2, otherwise chose the best fit individual (the winner) and terminate.

4.1. Data structure and generation of the initial population

The solution of the convolution Equation (16) is a data set containing the undistorted (instantaneous) kinetic response of the sample at the same time instants as the measured image function. The coded solution is exactly this data set, which means a vector containing floating point elements, each of them representing a measured value of the undistorted (instantaneous) kinetic response. In terms of GAs, this is a single haploid chromosome containing as much genes as there are data points measured. As each parent and each offspring is haploid, there is a haploid mechanism of reproduction to implement. There is no need to 'express' the genes as phenotypes; the chromosome already represents the solution itself.

Convolution results in a kind of a weighted moving average, which *widens* the signal temporally, *diminishes its amplitude*, makes its *rise and descent less steep*, and *smoothes out* its sudden steplike jumps. Accordingly, we started from the image itself to create the initial population and have implemented an operator to *compress* the image temporally, another to *enhance its amplitude*, a third one to *steepen its rise and decay*, and finally, one to *restitute the stepwise jump* by setting some leading elements of the data to zero.

All four operators—which we may call *creation operators*—are constructed to conduct a random search in a prescribed modification range. To this purpose, normally distributed random numbers are generated with given expectation and standard deviation for the factor of temporal compression, of amplitude enhancement, for increasing the steepness of rise and decay, and for the number of data to cut to zero at the leading edge of the data set. The whole resulting initial population is displayed graphically, along with the original image. The best individual and the result of the convolution of this individual with the spread function (the *reconvolved*), as well as the difference of this reconvolved set from the image is also displayed. If the reconvolved is too much different from the image, or if there are spurious oscillations present in the best individual, another initial population is created with different expectation and/or standard deviation parameters of the generation operators. The procedure is repeated until the user is content with the selected initial population.

Parameterisation of the creation operators can easily be done on an intuitive basis. The major point is that individuals should be without fluctuations. With a little experimentation, fairly good estimates of the deconvolved data set can be chosen as individuals of the initial population, which guarantees that any spurious oscillations would die out, and the population is driven towards a desired global optimum.

4.2. Parent selection and crossover

The quality of the deconvolved data set—an individual of the population—can be measured readily by the mean square error

(MSE) of the reconvolution, given by

$$\text{MSE} = \sqrt{\frac{\sum_{m=1}^N [(\hat{o} \otimes s)_m - i_m]^2}{N-1}} \quad (17)$$

where \hat{o} is the estimate of the deconvolved, i.e. the actual individual of the population, and N is the number of data in the image data set. GA literature suggests that some kind of *inverse* of this error should be used so that the resulting fitness function is normalised [28–30]. We implemented a dynamic scaling of fitness by adding the minimal MSE of the population in the denominator:

$$\text{fitness}_m = \frac{1}{\min(\text{MSE}) + \text{MSE}_m}, \quad (17)$$

which maintains the fitness values in the range from $1/(\min(\text{MSE}) + \max(\text{MSE}))$ to $1/(2 \min(\text{MSE}))$.

To choose parents for mating, we use stochastic sampling with replacement, implemented as a *roulette-wheel selection* [27–30], which imitates natural selection in real-world population dynamics. To have the offspring, *arithmetic crossover* of the parents is performed, which results in an offspring whose data points are the average of the corresponding parents' data. (Fitness-weighted averages did not result in an important difference concerning convergence and the quality of the winner.) This procedure of parent selection and crossover is made until the number of produced offspring becomes the same as the number of population minus one.

4.3. Mutation and selection of the new generation

The arithmetic crossover explores the potential solutions within the range represented by the initial population, but it cannot move the population out of this region. Mutation is used to further explore the fitness landscape of the solution space. This is also a crucial operator to avoid the usual noise amplification and low-frequency wavy behaviour. A 'smooth' mutation of neighbouring data points results in an effective smoothing of the mutated individuals after a few crossovers. It has been implemented as an addition of a randomly generated Gaussian to the actual data set. The expectation (centre), the standard deviation (width) and the amplitude of the additive Gaussian correction is randomly selected within a specified range, including both positive and negative amplitudes. (Leading zeros of the initial population get never changed by mutation, which is equivalent to a semi-finite-support constraint [14,31,32].) If there is a long tail of the kinetic response (e.g. due to largely different characteristic times involved in the reaction mechanism), its slow decrease can also be reconstructed by this mutation, even if the initial population had a much sharper decrease without a long tail.

There is another feature which proved to be useful; non-uniform mutation [29]. This is responsible for a fine-tuning of mutations so that it moves even a rather uniform and close to optimal population further towards the global optimum. If the mutation amplitude is small, the convergence at the beginning of the iteration is also small. A larger amplitude results in a faster convergence but makes the improvement of individuals quite improbable after the deviation of the solution from the optimum

is much less than the mutation amplitude. To get a closer match of the optimum, it is necessary to diminish the amplitude of the mutation as the number of generations increases, or with decreasing deviation from the optimum. We perform this adjustment by estimating the experimental error as the standard deviation of measured image data in the range where its values are more or less constant. (For example in the leading zero level of the signal.) Comparing this experimental error to the difference between the MSE of the fittest and the least fit individuals, the amplitude parameter of the Gaussian mutation is multiplied by the factor

$$f = 1 - e^{1 - \left(\frac{\text{MSE difference}}{\text{experimental error}}\right)^p} \quad (18)$$

This factor goes to zero as the MSE difference of the best fit and the least fit individuals goes to the experimental error. This correction also avoids too large modifications, resulting in a less noisy deconvolved data set. The higher the power p , the more enhanced is the tuning effect of the factor. To avoid problems arising from an overestimation of the experimental error, this factor f can be checked and set equal to a prescribed smallest value if the ratio in the exponent becomes too much close to one, or even less.

When the number of newly generated offspring equals the population number minus one, selection of the new generation is done. All the parents die out except for the best fit which also becomes member of the new generation. This selection method is called *single elitism* and guarantees a monotonous improvement of the best individual.

4.4. Termination and the choice of the winner

After each generation, the quality of individuals is evaluated by the MSE between image and reconvolved, as it is necessary to calculate the fitness. In addition, the Durbin–Watson (DW) statistics of the residual differences between these two data sets in the case of the best fit individual is also calculated [33–35]. The equivalent of the experimental error—the standard deviation of a few data of the image data set which can be considered constant—can be calculated similarly from the deconvolved data.

To terminate the iteration, we can use the criterion that the MSE between the image and the reconvolved data set of the best individual—the *winner*—should be less than or equal to the experimental error. However, it does not guarantee that the reconvolved solution closely matches the image; there might be some bias present in the form of low-frequency waviness. The DW statistics is a sensitive indicator of such misfits. For the large number of data in a kinetic trace (typically more than 200), its critical value for a test of random differences is around 2.0 [33–34], and it is typically much lower than that for a wavy set of differences. Thus we may either use a DW value close to 2.0 as a criterion, or combine the experimental error criterion with the DW criterion so that both of them should be fulfilled.

There are less specific GA properties that can also be used to stop the iteration. If the MSE of the best individual would not change for a prescribed number of generations, the algorithm might have converged. Similarly, if the difference between the MSE of the best fit and the least fit individual becomes less than the experimental error, we cannot expect too much change in the population due to mutations. However, the use of these criteria

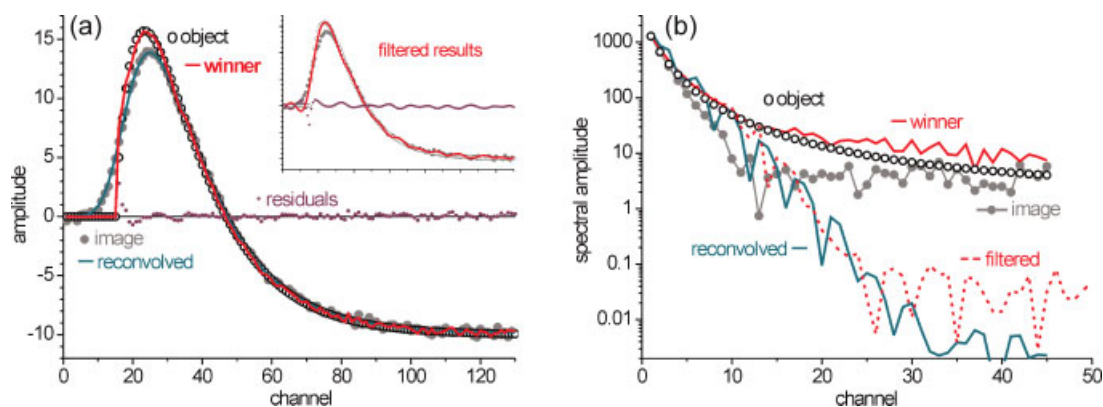


Figure 1. Deconvolution results for synthetic transient absorption data F3 with bleaching. (a) Time-domain representation showing the undistorted object (open circles), the synthetic image with added noise (full circles), the deconvolved data (solid curve close to the object), the reconvolution of the deconvolved data (solid curve close to the image) and the residual differences between image and reconvolved (dots). The inset shows deconvolution results obtained with a regularisation filter. (cf. Reference [14]) (b) Frequency-domain representation showing the amplitude spectra of the corresponding data using the same notation as in panel (a). The best result obtained with a regularisation filter is shown as a dashed curve.

only indicates that the GA itself has converged but it does not guarantee a satisfactory solution.

5. RESULTS AND DISCUSSION

We have implemented the GA described above as a package of user defined Matlab functions and scripts. All the input data including filenames and operator parameters are entered into a project descriptor text file. The output file contains the entire project descriptor, statistical evaluations, and all relevant results. In addition, there is a four-panel figure displayed, containing most of the results for immediate graphical evaluation.

To test the performance of the algorithm, we used the same synthetic data calculated for a simple consecutive reaction containing two first-order steps, as in previous publications [12–14]. These three data sets were chosen so that they mimic typical transient absorbance curves, including a completely decomposing reactant (hereafter: F1) along with two transients; one containing also a product with positive remaining ΔOD (F2) and another with bleaching, i.e. with negative remaining ΔOD (F3). Characteristic times were set at 200 and 500 fs, and calculated data were convolved with a 255 fs fwhm effective pulse. Kinetic responses were sampled at 30 fs intervals, and a normally distributed noise of 2% of their maximum amplitude was added. However, as recent measurements in fluorescence detection also explored extremely short characteristic times with simultaneous long-time components [36,37], we also tested a synthetic data set mimicking this situation, with the actual fluorescence intensity I_f calculated as

$$I_f = 0.9 e^{-\frac{30fs}{\tau}} + 0.1 e^{-\frac{150fs}{\tau}} \quad (19)$$

This function was convolved with an effective pulse of 330 fs fwhm, sampled at 11 fs intervals, and a normally distributed noise of 0.5% of maximum intensity was added, which reflects typical experimental conditions [36,37]. While the data set with bleaching necessitates the most careful transformations using the creation operators, this double fluorescence decay challenges the power of the algorithm to reconstruct an extremely large stepwise jump

followed immediately by a steep decay with a tenfold shorter characteristic time than that of the IRF, then ending in a long tail.

5.1. Test results for synthetic data

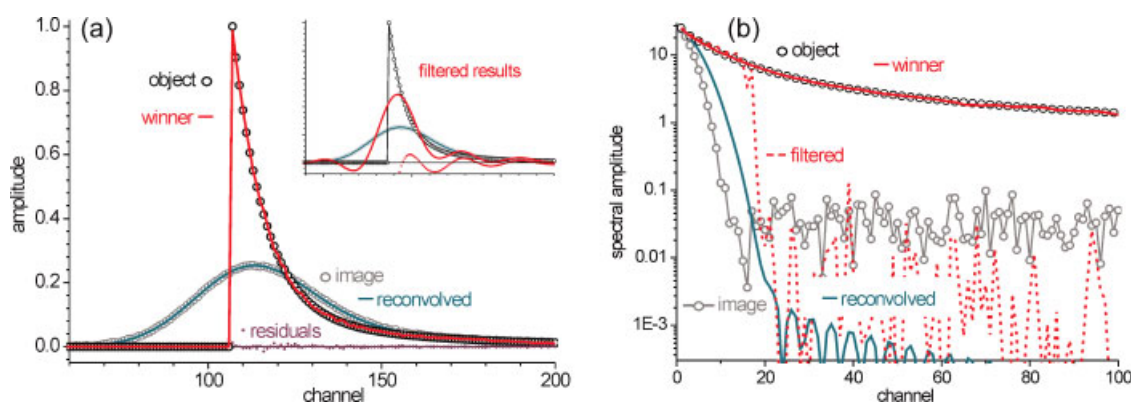
Figure 1a shows the best result obtained for a highly non-periodic synthetic data set comprising both positive and negative data, a slight initial stepwise jump and a remaining bleaching. As it can be seen, there is still a slight wavy bias at a few data points immediately after the steplike initial rise, but its amplitude rapidly diminishes within the experimental noise, and further on it becomes rather a random noise without bias. It can be compared to the best inverse filtered result [14] (inset), where a more substantial wavy behaviour is present along the whole deconvolved curve. (It should be noted that a slight initial wavy bias is usually present even in the case of reconvolution using a known model function.) We can judge the superior quality of the deconvolution result obtained using the GA comparing the spectral amplitudes of the data in the frequency domain (Figure 1b). The deconvolved (winner) has only slightly larger high-frequency components than the original (noise-free) object function (indicating that the winner data set also contains noise which is not present in the displayed—noiseless—object data), so the deconvolved signal has practically been reconstructed in the entire frequency range. In contrast to this frequency behaviour, the best inverse filtered result obtained in Reference [14] has a frequency spectrum where the amplitude of the deconvolved data sharply diminishes after channel 10 with respect to the object (dashed curve in Figure 1b). The frequency damping is about 100-fold above channel 20 and at higher frequencies. Results obtained with the best iterative methods are quite similar; there is always an important loss in high-frequency components during deconvolution [14].

Table I shows some quantitative statistical data to compare the quality of different deconvolution methods. The MSE of the deconvolved data set resulting from the GA is always substantially less than the MSE of the deconvolved data set resulting from reconvolution, though this latter explicitly includes the known model function used to constrain deconvolution. A remarkable feature is that—while F2 and F3 obtained with GA have roughly twice as large an MSE as that of the image with

Table I. Comparison of statistics characterising the quality of deconvolution for synthetic transient absorption data

Deconvolution method	Statistics ^a	F1	F2	F3
Reconvolution (using known model)	MSE	0.260	0.661	0.727
	DW	0.587	1.535	1.882
Bayesian iteration of reblurred data	MSE	2.392	1.045	0.714
	DW	1.191	0.225	0.311
Inverse filtering (using Wiener filter)	MSE	2.320	1.018	0.707
	DW	1.156	0.214	0.301
Genetic algorithm	MSE	0.158	0.446	0.324
	DW	0.893	1.841	1.284
MSE of image with respect to reconvolved		0.248	0.202	0.203

MSE: mean square error; DW: Durbin–Watson.
^a Both MSE and DW refer to differences of the deconvolved data set with respect to the noiseless object.

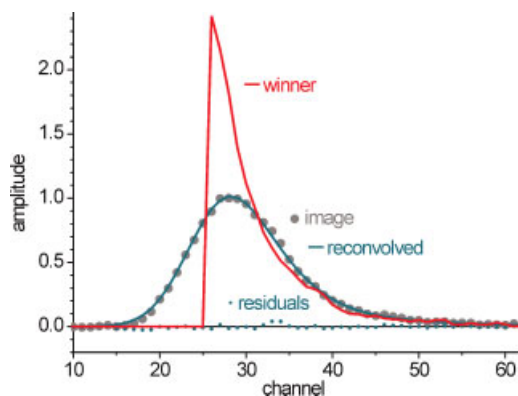
**Figure 2.** Deconvolution results for synthetic transient fluorescence data, using the same notation as in Figure 1. (a) Time-domain data. (b) Frequency-domain representation showing the amplitude spectra. Note the complete recovery of the frequencies of the object data set.

respect to reconvolved—F1 obtained with GA has only about 60% of the MSE of image with respect to reconvolved. This indicates that GA is extremely powerful as a deconvolution method if there is a steplike increase in the kinetic function, as in the case of a reactant-like species—it even smoothes the noise in the measured (image) data during deconvolution.

DW statistics also reveal the superiority of the GA deconvolution method. Actual realisations of this statistics are quite closer to the limiting value indicating no serial correlation (2.0) for F1 and F2, than for the reconvolution results. The case of F3 is different, as the DW statistics is based on neighbouring MSE differences, and the MSE is rather low for the deconvolution of the image originating from F3; i.e. the somewhat lower value of the DW statistics is a result of a substantially lower MSE.

Figure 2 shows the deconvolution results of synthetic fluorescence data. Though the image function is periodic in this case—as in many real-life experimental data—it has a large steplike jump from its minimal to its maximal value within one channel. This jump is also characteristic in most of the real-life experiments. The sudden steplike change could not have been reconstructed either with inverse filtering [13,38], or with iterative deconvolution methods [14,38]; the sharp peak at the initial jump had always become slightly curved and its amplitude diminished, having resulted in a considerable low-frequency wavelike

oscillation before and after the maximum (see inset). As it can be seen from the figure, the sudden steplike jump is completely recovered by the GA deconvolution, without any bias in the form of low-frequency oscillations. The residual differences between the image and the reconvolved look completely random, and the

**Figure 3.** Deconvolution results for experimental transient fluorescence data of adenosine monophosphate in aqueous solution obtained by

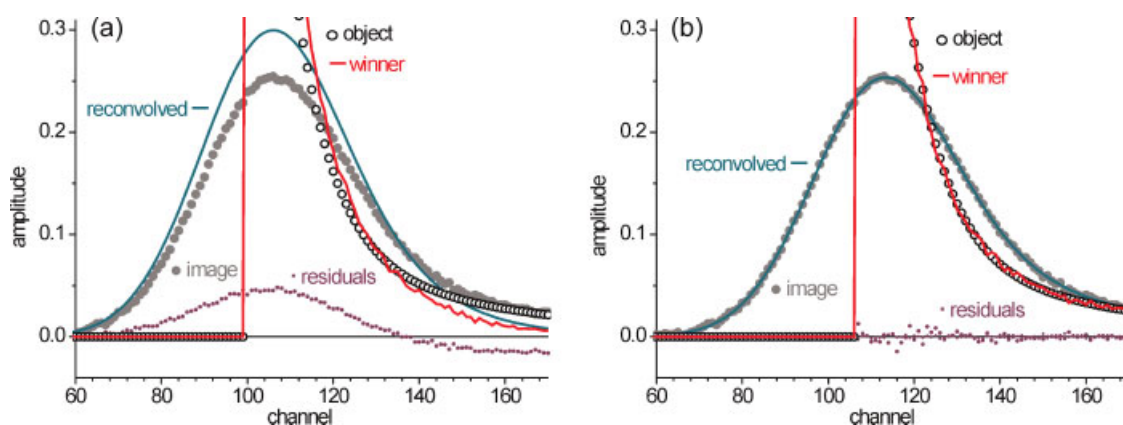


Figure 4. Deconvolution of the same data as shown in Figure 2. with an enlarged amplitude scale. (a) The best individual of the initial population (i.e. first generation, no iteration). (b) Results starting from the same initial population but after 2000 generations.

frequency spectrum of the deconvolved (winner) is also identical to that of the object. The reconvolved curve has larger low frequency amplitudes but much smaller high frequency amplitudes than the image data. Accordingly, in the time domain, the reconvolved data set is markedly smoother than the original image.

Quantitative statistics also support the surprisingly good quality of the GA deconvolution. MSE of the deconvolved data with respect to the noiseless object is 36 times less than for the best inverse filtered result, and the DW statistics is almost three times greater (1.791) than that of the inverse filtered deconvolved (0.619), though the former is normalised to the 36 times smaller MSE.

5.2. Test results for experimental data

Test results for an experimental transient fluorescence data set are shown in Figure 3. These data are collected at 33.33 fs intervals per channel, and the experimentally determined effective pulse has a width of 270 fs fwhm, i.e. 8 channels. The expected sudden jump is fully recovered, and the residual error of the reconvolved data with respect to the measured image is almost completely random. The only exception can be observed from channel 31 to 36, where the residual error has a slight hump-like bias. This is the consequence of a marked shoulder-like feature in the measured image data around the corresponding delay times which is either a kinetic effect, or some experimental artefact which is reflected also in the deconvolved data set. Even with this small discrepancy, the deconvolved curve can be considered as a successful reconstruction of an instantaneous fluorescence response. The amplitude spectrum of the winner (not shown) displays a quite similar behaviour as in the case of the synthetic fluorescence data in Figure 2(b); the amplitude of the winner at higher frequencies is larger by a factor of 20 than that of the image.

5.3. Some remarks on mutations used

It is worth mentioning the ability of mutations to arrange for the mismatch of long-tailed data sets. As already pointed out, in case if there are largely different characteristic times involved in the kinetics studied (30 and 150 fs in the case of the synthetic fluorescence data shown in Figure 2), one of the operators to create the initial individuals, which increases the decay rate of the image data set, provides individuals whose decay is so sharp that

their long tail is largely suppressed. Though this is necessary to reconstruct the sharp decay following the step-like jump due to the short characteristic time, the missing tail results in a considerable mismatch of the reconvolved and the image data. With a little experimentation, it can easily be seen that a satisfying solution can be achieved increasing the initial amplitude and letting to form a lower tail while creating the initial individuals, leaving the tail correction to the mutations of subsequent generations.

To illustrate the success of this procedure, Figure 4 shows the tail part of the deconvolved set for the same data as seen in Figure 2. In panel (a) we can see the best individual of the initial population, while panel (b) shows the winner after 2000 generations. As crossovers cannot change the values of the alleles (data at a given time channel) out of the region already contained in the initial population, it is the mutations that 'fill up' the gap in the missing tail and 'push down' the values that are too high at the maximum. The result of the simultaneous change of neighbouring channels using the random Gaussian is a smoothed deconvolved with an excellent fit.

Another feature worth mentioning is the effect of the non-uniform mutation. It allows large mutations at the beginning of the iteration but diminishes mutation amplitude when the MSE differences within the population become close to the experimental error in the measured data. As a consequence, low-frequency waviness is further suppressed and mutations lead to a smoother deconvolved data set. A value of the exponent $p = 1.5$ proved to be efficient when deconvolving the data shown here. The number of necessary generations to reach an optimal solution is usually a few thousands, but it takes only a couple of minutes even on a moderately fast desktop PC.

6. CONCLUSIONS

During the last decade, there have been a few attempts to apply a GA for deconvolution purposes with considerable success. The modified GA for the model-free deconvolution of transient ultrafast kinetic signals described here uses the measured transient data as chromosomes containing floating point genes, a careful generation of initial individuals followed by an evolution combining crossing, selection and mutation operators leading to unprecedented results concerning the quality of the deconvolved data.

The main shortcoming of deconvolution methods used previously to transient kinetic data was the limited reconstruction capacity of the high-frequency components of the transient signal and a low-frequency wavy behaviour of the deconvolved data. To overcome these shortcomings, we have modified the classical GA by introducing a careful generation of the initial population and a special mutation changing neighbouring genes simultaneously. Due mainly to the operator which cuts some leading data of the signal to zero, and to the mutation procedure that maintains these leading zeros, the high-frequency part can be fully reconstructed. This results in a deconvolved data set with the expected sudden steplike increase. The waviness is avoided by applying the smooth arithmetic mutation of neighbouring genes instead of single point mutations, along with a dynamically changing mutation that fine-tunes the amplitude of the changes according to the closeness of the population to the optimal solution.

Deconvolution using this modified GA outperforms existing algorithms and produces unprecedented quality of the reconstructed original signal for highly non-periodic transient absorption as well as highly distorted steplike fluorescence traces. Results on real-life experimental data also support the applicability of the proposed deconvolution method.

Further work is in progress to explore the power of the applied GA, and to develop a user-friendly, interactive graphical interface that largely facilitates the use of the deconvolution code. An attempt is also made to allow a fully automated routine deconvolution with the least possible intervention of the user.

Acknowledgements

The author thanks Thomas Gustavsson and Ákos Bányász for experimental data and detailed information of the experimental conditions. Péter Pataki is acknowledged for his contribution to the Matlab code. The financial support of the Balaton exchange program (contract no. 11038YM) and the National Research Fund of Hungary under contract no. OTKA T 048725 is gratefully acknowledged.

REFERENCES

1. Burger HC, van Cittert PH. Wahre und scheinbare Intensitätsverteilung in Spektrallinien. *Z. Phys.* 1932; **79**: 722–730.
2. Fell AF, Scott HP, Gill R, Moffat AC. Novel techniques for peak recognition and deconvolution by computer-aided photodiode array detection in high-performance liquid-chromatography. *J. Chromatogr.* 1983; **282**: 123–140.
3. Mitra S, Bose T. Adaptive digital filtering as a deconvolution procedure in multiinput chromatography. *J. Chromatogr. Sci.* 1992; **30**: 256–260.
4. Chase WJ, Hunt JW. Solvation time of electron in polar liquids – water and alcohols. *J. Phys. Chem.* 1975; **79**: 2835–2845.
5. Pananakis D, Abel EW. A comparison of methods for the deconvolution of isothermal DSC data. *Thermochim. Acta.* 1998; **315**: 107–119.
6. Gobbel GT, Fike JR. A deconvolution method for evaluating indicator-dilution curves. *Phys. Med. Biol.* 1994; **39**: 1833–1854.
7. McKinnon AE, Szabo AG, Miller DR. Deconvolution of photoluminescence data. *J. Phys. Chem.* 1977; **81**: 1564–1570.
8. O'Connor DV, Ware WR, André JC. Deconvolution of fluorescence decay curves – critical comparison of techniques. *J. Phys. Chem.* 1979; **83**: 1333–1343.
9. Bernstein RB, Zewail AH. Special report – real-time laser femtochemistry – viewing the transition from reagents to products. *Chem. Eng. News* 1988; **66**: 24–43.
10. Zewail AH. Laser femtochemistry. *Science* 1988; **242**: 1645–1653.
11. Simon JD (ed.). *Ultrafast Dynamics of Chemical Systems*. Kluwer Academic Publishers: Dordrecht, 1994.
12. Bányász Á, Mátyus E, Keszei E. Deconvolution of ultrafast kinetic data with inverse filtering. *Radiat. Phys. Chem.* 2005; **72**: 235–242.
13. Bányász Á, Dancs G, Keszei E. Optimisation of digital noise filtering in the deconvolution of ultrafast kinetic data. *Radiat. Phys. Chem.* 2005; **74**: 139–145.
14. Bányász Á, Keszei E. Nonparametric deconvolution of femtosecond kinetic data. *J. Phys. Chem. A* 2006; **110**: 6192–6207.
15. Johnson EG, Abushagur MAG. Image deconvolution using a micro genetic algorithm. *Opt. Commun.* 1997; **140**: 6–10.
16. Chen YW, Nakao Z, Arakaki K, Tamura S. Blind deconvolution based on genetic algorithms. *IEICE T. Fund. Elect.* 1997; **E80A**: 2603–2607.
17. Yin HJ, Hussain I. Independent component analysis and nongaussianity for blind image deconvolution and deblurring. *Integr. Comput.-Aid. E.* 2008; **15**: 219–228.
18. Sprzechak P, Moravski RZ. Calibration of a spectrometer using a genetic algorithm. *IEEE T. Instrum. Meas.* 2000; **49**: 449–454.
19. Tripathy SP, Sunil C, Nandy M, Sarkar PK, Sharma DN, Mukherjee B. Activation foils unfolding for neutron spectrometry: comparison of different deconvolution methods. *Nucl. Instrum. Meth. A* 2007; **583**: 421–425.
20. Vivo-Truyols G, Torres-Lapasio JR, Garrido-Frenich A, Garcia-Alvarez-Coque MC. A hybrid genetic algorithm with local search I. Discrete variables: optimisation of complementary mobile phases. *Chemometr. Intell. Lab.* 2001; **59**: 89–L 106.
21. Vivo-Truyols G, Torres-Lapasio JR, Garrido-Frenich A, Garcia-Alvarez-Coque MC. A hybrid genetic algorithm with local search II. Continuous variables: multibatch peak deconvolution. *Chemometr. Intell. Lab.* 2001; **59**: 107–120.
22. Wasim M, Brereton RG. Hard modeling methods for the curve resolution of data from liquid chromatography with a diode array detector and on-flow liquid chromatography with nuclear magnetic resonance. *J. Chem. Inf. Model.* 2004; **46**: 1143–1153.
23. Mico-Tormos A, Collado-Soriano C, Torres-Lapasio JR, Simo-Alfonso E, Ramis-Ramos G. Determination of fatty alcohol ethoxylates by derivatisation with maleic anhydride followed by liquid chromatography with UV-vis detection. *J. Chromatogr.* 2008; **1180**: 32–41.
24. Madden FN, Godfrey KR, Chappell MJ, Hovorka R, Bates RA. A comparison of six deconvolution techniques. *J. Pharmacokinet. Biop.* 1996; **24**: 283–299.
25. Donoho DL, Stark PB. Uncertainty principle and signal recovery. *SIAM J. Appl. Math.* 1989; **49**: 906–931.
26. Jansson PA. (ed.). *Deconvolution of Images and Spectra*, 2nd edn. Academic Press: San Diego, US, 1997.
27. Holland JH. *Adaptation in Natural and Artificial Systems*. University of Michigan Press: Ann Arbor, 1975.
28. Mitchell M. *An Introduction to Genetic Algorithms*. MIT Press: Cambridge, Mass, 1996.
29. Michalewicz Z. *Genetic Algorithms + Data Structures = Evolution Programs*. Springer: Berlin, 1992.
30. Busetto F. *Genetic Algorithms Overview*. <http://www.scribd.com/doc/396655/Genetic-Algorithm-Overview> (30 August 2008).
31. Jansson PA. (ed.). *Deconvolution of Images and Spectra*, 2nd edn. Academic Press: San Diego, 1997.
32. Schafer RW, Merserau RM, Richards MA. Constrained iterative restoration algorithms. *Proc. IEEE* 1981; **69**: 432–450.
33. Durbin J, Watson GS. Testing for serial correlation in least squares regression I. *Biometrika* 1950; **37**: 409–428.
34. Durbin J, Watson GS. Testing for serial correlation in least squares regression II. *Biometrika* 1950; **38**: 159–178.
35. Turi L, Holpár P, Keszei E. Alternative mechanisms for solvation dynamics of laser-induced electrons in methanol. *J. Phys. Chem. A* 1997; **101**: 5469–5476.
36. Bányász Á, Gustavsson T, Keszei E, Improta R, Markovitsi D. Effect of amino substitution on the excited state dynamics of uracil. *Photoch. Photobiol. Sci.* 2008; **7**: 765–768.
37. Gustavsson T, Bányász Á, Lazzarotto E, Markovitsi D, Scalmani G, Frisch MJ, Barone V, Improta R. Singlet excited-state behavior of uracil and thymine in aqueous solution: a combined experimental and computational study of 11 uracil derivatives. *J. Am. Chem. Soc.* 2006; **128**: 607–619.
38. Bányász Á. Model-free deconvolution of ultrafast kinetic data and the study of singlet excited states of uracil derivatives. *PhD Thesis*, Eötvös Loránd University, Budapest, 2006.